Giant Collective Spin-Orbit Field in a Quantum Well: Fine Structure of Spin Plasmons

F. Baboux,[1,*] F. Perez,[1] C. A. Ullrich,[2] I. D'Amico,[3] J. Gómez,[1,†] and M. Bernard[1]

[1]*Institut des Nanosciences de Paris, CNRS/Université Paris VI, Paris 75005, France*
[2]*Department of Physics and Astronomy, University of Missouri, Columbia, Missouri 65211, USA*
[3]*Department of Physics, University of York, York YO10 5DD, United Kingdom*

(Received 13 July 2012; published 15 October 2012)

We employ inelastic light scattering with magnetic fields to study intersubband spin plasmons in a quantum well. We demonstrate the existence of a giant collective spin-orbit (SO) field that splits the spin-plasmon spectrum into a triplet. The effect is remarkable as each individual electron would be expected to precess in its own momentum-dependent SO field, leading to D'yakonov-Perel' dephasing. Instead, many-body effects lead to a striking organization of the SO fields at the collective level. The macroscopic spin moment is quantized by a uniform collective SO field, five times higher than the individual SO field. We provide a momentum-space cartography of this field.

DOI: 10.1103/PhysRevLett.109.166401 PACS numbers: 71.70.Ej, 72.25.Rb, 73.21.−b, 78.30.−j

Spin-orbit (SO) coupling arises from relativity: the spin of an electron moving at a velocity $\mathbf{v}$ in a static electric field $\mathbf{E}$ sees a magnetic field $\mathbf{B}_{\mathrm{SO}} = -(1/c^2)\mathbf{v} \times \mathbf{E}$ (c is the speed of light) [1]. This magnetic field splits the energy levels of atoms, giving rise to their fine structure [2]. For an ensemble of itinerant electrons in solids, such a simple quantizing effect cannot be expected because of the distribution of velocities. Momentum-dependent SO fields cause each individual electronic spin to precess with its own axis, which destroys spin coherence (D'yakonov-Perel' [DP] decoherence [3]). This sets practical limitations on many proposed applications in emerging quantum technologies such as spintronics [4–8].

However, this DP picture is appropriate only for situations where the macroscopic spin is carried by individual electrons, which is often the case [5,8–11]. Here, we demonstrate that Coulomb interaction, which plays a central role in collective spin excitations, can drastically modify this picture, and give rise to macroscopic quantum objects. We will focus on intersubband (ISB) spin plasmons in doped semiconductor quantum wells, which, as we shall see, are ideal to study the interplay of SO coupling and Coulomb interactions.

In a III–V quantum well, internal SO fields arise from the lack of an inversion center of the crystalline unit cell and from an asymmetric confining potential [12], referred to as Dresselhaus [13] and Rashba [14] fields, respectively. Hence, a conduction electron with momentum $\mathbf{k}$, moving in the plane of a [001]-oriented quantum well, experiences a SO magnetic field

$$\mathbf{B}_{\mathrm{SO}}(\mathbf{k}) = \frac{2\alpha}{g\mu_{\mathrm{B}}}\begin{pmatrix} k_y \\ -k_x \end{pmatrix} + \frac{2\beta}{g\mu_{\mathrm{B}}}\begin{pmatrix} k_x \\ -k_y \end{pmatrix}, \qquad (1)$$

(to lowest order in $\mathbf{k}$) for coordinate systems with $\hat{x} \parallel [100]$ and $\hat{y} \parallel [010]$. Here, α and β are the Rashba and linear Dresselhaus coupling constants [12], respectively, g is the electron g factor, and μ_{B} the Bohr magneton. $\mathbf{B}_{\mathrm{SO}}$ produces an intrinsic $\mathbf{k}$-dependent spin splitting [9,10] and a $\mathbf{k}$-dependent spin orientation [6,15] of single-electron conduction states.

In such a system, electrons can exhibit collective spin dynamics when excited from the first to the second subband of the quantum well. These so-called ISB spin plasmons, which arise from Coulomb interactions, are energetically well separated from the continuum of ISB single-particle excitations [16,17]. In the absence of a transferred momentum $\mathbf{q}$ and external magnetic field $\mathbf{B}_{\mathrm{ext}}$, time reversal symmetry, together with the [001]-axis symmetry of the quantum well, average out the $\mathbf{k}$-dependent $\mathbf{B}_{\mathrm{SO}}$. Hence, no macroscopic SO force is acting on the electron gas, and the spin plasmons are degenerate. However, when transferring an in-plane momentum $\mathbf{q}$ to the electron gas, the translation symmetry is broken, and $\mathbf{B}_{\mathrm{SO}}(\mathbf{k})$ does not average out anymore.

In this situation, it has been predicted [18,19] that despite the spread of $\mathbf{B}_{\mathrm{SO}}(\mathbf{k})$, a collective SO magnetic field $\mathbf{B}_{\mathrm{SO}}^{\mathrm{coll}}(\mathbf{q})$ emerges, splitting the spin plasmon branch into three modes [Fig. 1(a)]: one longitudinal oscillation mode ($m_{\parallel}$) and two transverse precession modes (m_+ and m_-). In the present work, we focus on these transverse modes, whose frequencies are shifted in opposite directions by SO coupling. We propose that due to Coulomb interaction, these modes behave as macroscopic quantum objects, characterized by a collective spin magnetic moment $\mathbf{M}$ and, thus, subject to an interaction energy $W(\mathbf{q}) = -\mathbf{M} \cdot \mathbf{B}_{\mathrm{SO}}^{\mathrm{coll}}(\mathbf{q})$. Within this framework, the downward (upward) energy shift of the m_+ (m_-) mode is explained by its projected magnetic moment being parallel (antiparallel) to the quantizing field $\mathbf{B}_{\mathrm{SO}}^{\mathrm{coll}}(\mathbf{q})$ [Fig. 1(c), left]. Then, in the presence of an external magnetic field, we expect both fields to superpose [5,11] [Fig. 1(c), right] and the interaction energy to become

$$W(\mathbf{q}) = -\mathbf{M} \cdot (\mathbf{B}_{\mathrm{SO}}^{\mathrm{coll}}(\mathbf{q}) + \mathbf{B}_{\mathrm{ext}}). \qquad (2)$$

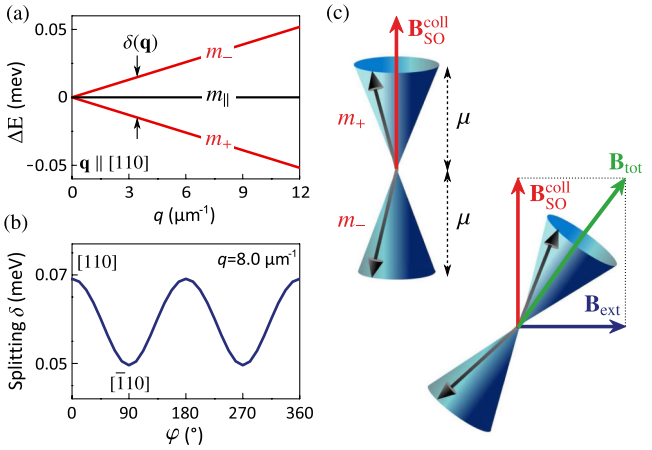

FIG. 1 (color online). Fine structure model of ISB spin plasmons. (a) Threefold splitting, induced by SO coupling, of the ISB spin-plasmon modes. ΔE denotes the difference of the mode energies with and without SO coupling, calculated for the studied GaAs quantum well, and q is the magnitude of the plasmon momentum (here $\mathbf{q} \parallel [110]$). The splitting δ between the transverse $m_\pm$ modes is almost linear in q. (b) For a fixed $q = 8.0\ \mu\mathrm{m}^{-1}$, calculated modulation of the splitting δ with the in-plane orientation of $\mathbf{q}$, labeled by the angle φ to [110]. (c) Sketch of the proposed interpretation of the transverse ISB spin plasmons $m_\pm$, as the precession of antiparallel μ collective magnetic moments about $\mathbf{B}_{\mathrm{SO}}^{\mathrm{coll}}$ at zero external field (left), and about the superposition $\mathbf{B}_{\mathrm{SO}}^{\mathrm{coll}} + \mathbf{B}_{\mathrm{ext}}$ when an external magnetic field $\mathbf{B}_{\mathrm{ext}}$ is applied (right).

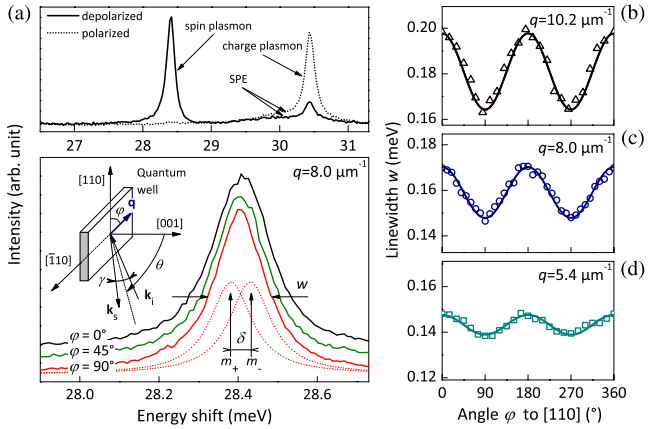

FIG. 2 (color online). Anisotropic splitting of the ISB spin-plasmon modes. (a) Top panel: Inelastic light-scattering spectrum of the ISB excitations, in polarized (dashed line) and depolarized (solid line) geometry. Bottom panel: Depolarized spectra obtained at fixed $q = 8.0\ \mu\mathrm{m}^{-1}$, by varying the in-plane angle φ measured from [110] (vertical offset for clarity). The single, quasi-Lorentzian peak observed is the sum of two Lorentzians (red dashed lines for the $\varphi = 90°$ spectrum) of same amplitude and linewidth, corresponding to the transverse spin-plasmon modes m_+ and m_- split by an amount δ. Inset: Scattering geometry showing angle definitions; $\mathbf{k_i}$ and $\mathbf{k_s}$ are the incoming and scattered light wave vectors. (b–d) Variation of the linewidth w with φ for $q = 10.2$, 8.0, and 5.4 $\mu\mathrm{m}^{-1}$ respectively. Lines: Theory (see text).

We will demonstrate that this fine structure model correctly captures the physics of the ISB spin plasmons.

We carry out inelastic light-scattering measurements in a [001]-oriented, asymmetrically modulation-doped GaAs/AlGaAs quantum well. The electron density is $2.3 \times 10^{11}\ \mathrm{cm}^{-2}$, and the mobility $2 \times 10^7\ \mathrm{cm}^2\,\mathrm{V}^{-1}\,\mathrm{s}^{-1}$ at the working temperature $T \simeq 2$ K (superfluid helium) [20]. Inelastic light-scattering [16,21] is a powerful tool to study spin excitations at a given transferred momentum $\mathbf{q}$ [Fig. 2(a), inset] [20]. Standard selection rules [16] allow us to address the various types of ISB excitations individually. As shown in the spectra of Fig. 2(a) (top), the charge plasmon is observed only when the incident and scattered photon have parallel polarizations (polarized geometry), while the spin plasmon appears when they have orthogonal polarizations (depolarized geometry). The single-particle excitations continuum appears in both configurations (here as a shoulder of the charge plasmon peak). From now on we focus on the spin-plasmon peak, obtained in the depolarized geometry where only the transverse modes m_+ and m_- are probed. Typical spectra, taken in the absence of an external magnetic field, are presented in Fig. 2(a) (bottom). These are obtained for a momentum of fixed magnitude $q = 8.0\ \mu\mathrm{m}^{-1}$, but various in-plane orientations, labeled by the angle φ between $\mathbf{q}$ and the [110] direction of the quantum well. The spectra exhibit a single, quasi-Lorentzian peak of full width at half-maximum (FWHM) w; when plotting w for various φ [Fig. 2(c)], w is modulated quasisinusoidally with a period π. This modulation is a characteristic of the twofold symmetry of SO splitting [Fig. 1(b)], with a maximum along [110] ($\varphi = 0°$) and a minimum along [$\bar{1}$10] ($\varphi = 90°$). Furthermore, as seen in Figs. 2(b)–2(d), the amplitude of the modulation decreases with decreasing q, in agreement with Fig. 1(a). Both characteristics confirm the SO origin of the modulation. This suggests that the observed Raman line is the sum of two Lorentzian peaks corresponding to the transverse spin-plasmon modes m_+ and m_-, split by δ [Fig. 2(a), red dashed lines]. By independently determining the FWHM of the latter peaks, we will extract the splitting $\delta(\mathbf{q})$ by deconvolution, and demonstrate the consistency of our model.

We determine the collective SO field $\mathbf{B}_{\mathrm{SO}}^{\mathrm{coll}}(\mathbf{q})$ by applying an external magnetic field $\mathbf{B}_{\mathrm{ext}}$. Since $\mathbf{B}_{\mathrm{SO}}^{\mathrm{coll}}(\mathbf{q})$ is expected [19] to lie in the plane of the quantum well for our [001]-oriented sample, $\mathbf{B}_{\mathrm{ext}}$ will be applied in the well plane (quasi-Voigt geometry). If the spin-plasmon moment $\mathbf{M}$ is of quantum nature, its energy levels will be quantized by the total field $\mathbf{B}_{\mathrm{tot}} = \mathbf{B}_{\mathrm{SO}}^{\mathrm{coll}}(\mathbf{q}) + \mathbf{B}_{\mathrm{ext}}$. Following Eq. (2), the splitting δ will then be given by

$$\delta = 2\mu B_{\mathrm{tot}} = 2\mu\sqrt{(B_{\mathrm{ext}} + \mathbf{B}_{\mathrm{SO}}^{\mathrm{coll}} \cdot \mathbf{u})^2 + (\mathbf{B}_{\mathrm{SO}}^{\mathrm{coll}} \times \mathbf{u})^2}, \tag{3}$$

where μ is the quantized value of the spin-plasmon magnetic moment and $\mathbf{u}$ is a unit vector parallel to the direction of $\mathbf{B}_{\text{ext}}$.

For a given $\mathbf{q}$, we record a series of spectra at varying B_{ext}, with $\mathbf{B}_{\text{ext}}$ applied successively along two crossed directions: $\mathbf{B}_{\text{ext}} \perp \mathbf{q}$ and $\mathbf{B}_{\text{ext}} \parallel \mathbf{q}$. Figures 3(a) and 3(b), respectively, present the composite linewidth w as a function of B_{ext} for these two configurations. The various plots are obtained for fixed $q = 8.0\ \mu\text{m}^{-1}$, and a set of eight angles φ, spaced by 22.5° within a period π. Each plot exhibits a clear minimum for a certain value of B_{ext} and is symmetric with respect to that minimum.

According to Eq. (3), each minimum corresponds to the situation where $\mathbf{B}_{\text{ext}}$ exactly cancels the component of $\mathbf{B}_{\text{SO}}^{\text{coll}}(\mathbf{q})$ parallel to it, $B_{\text{ext}} = -\mathbf{B}_{\text{SO}}^{\text{coll}} \cdot \mathbf{u}$. Using this criterion, we extract the component $B_{\text{SO},\parallel}^{\text{coll}}$ of the collective SO field parallel to $\mathbf{q}$ from the plots of Fig. 3(a) and the perpendicular component $B_{\text{SO},\perp}^{\text{coll}}$ from the plots of Fig. 3(b). Figure 4(a) presents the values for $B_{\text{SO},\parallel}^{\text{coll}}$ (filled circles) and $B_{\text{SO},\perp}^{\text{coll}}$ (open circles). We find that $B_{\text{SO},\parallel}^{\text{coll}}$ is antisymmetric about the $[\bar{1}10]$ direction ($\varphi = 90°$) and $B_{\text{SO},\perp}^{\text{coll}}$ is symmetric.

To push the analysis further, we need experimental access to the SO splitting δ. This can be done by determining the linewidth of the $m_{\pm}$ modes [see Fig. 2(a)]. The latter is inferred from the zero external field and zero momentum value of the FWHM w of the composite peak (not shown), since in that case we expect the splitting δ to vanish [see Fig. 1(a)] and both peaks to lie perfectly on top of each other. This yields 0.124 ± 0.005 meV.

This linewidth value can be compared to theory. ISB spin plasmons are expected to be immune against DP dissipation [18,19]. Thus, owing to the very high mobility of the sample and the low working temperature, we expect the linewidth to be dominated by an intrinsic many-body effect, the spin Coulomb drag (SCD) [22–24]. The SCD is caused by a friction of Coulomb origin between carriers of opposite spin moving with different momenta. The ISB spin plasmon, where spin densities oscillate out of phase along the growth axis, provides an optimal scenario for the SCD [23]. A calculation of the corresponding linewidth within a local-density approximation yields an SCD linewidth of the order of a fraction of an meV, confirming that the dominant dissipation source is the SCD. As the latter is mainly due to the out-of-plane spin density oscillation, its $\mathbf{q}$ dependence, for $\mathbf{q}$ much smaller than the Fermi momentum, is weak and only to second order. Hence, we deconvolute all the $w(B_{\text{ext}})$ curves using the experimentally determined 0.124 meV.

Figure 4(e) presents $\delta(B_{\text{ext}})$ (symbols as in Fig. 3), obtained by deconvolution of the data of Fig. 3(a). Using Eq. (3), we can now evaluate the collective magnetic moment of the spin plasmons as $\mu = \delta(B_{\text{ext}} = 0)/(2|\mathbf{B}_{\text{SO}}^{\text{coll}}|)$. This ratio is plotted in Fig. 4(b) (squares) for the various φ probed. It appears constant with φ within the experimental error. We deduce $\mu = 28.8 \pm 0.7\ \mu\text{eV T}^{-1} = (0.50 \pm 0.01)\mu_{\text{B}}$.

The consistency of our interpretation of the data with the model of Eq. (3) is demonstrated in Fig. 4(e), which compares the experimental data points for $\delta(B_{\text{ext}})$ with the relation $\delta(B_{\text{ext}}) = 2\mu\sqrt{(B_{\text{ext}} + B_{\text{SO},\parallel}^{\text{coll}})^2 + B_{\text{SO},\perp}^{\text{coll}\ 2}}$ (lines), using the previously determined values of $B_{\text{SO},\parallel}^{\text{coll}}$, $B_{\text{SO},\perp}^{\text{coll}}$, and μ. An excellent agreement is found without introducing any fitting parameters.

We further validate our model by checking the q dependence of μ. We repeat the same experimental procedure for other values of q. Figure 4(c) presents the values of the minimum ($\varphi = 90°$, open diamonds) and maximum

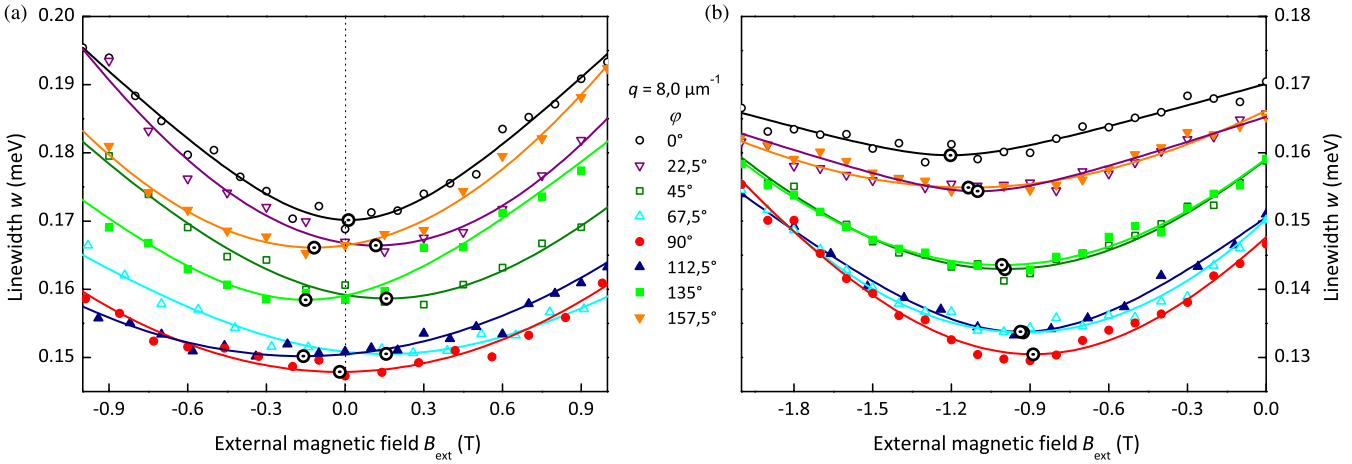

FIG. 3 (color online). Variation of the composite linewidth w with the external magnetic field $\mathbf{B}_{\text{ext}}$. (a) $w(B_{\text{ext}})$ plots obtained in the configuration $\mathbf{B}_{\text{ext}} \parallel \mathbf{q}$ for a fixed $q = 8.0\ \mu\text{m}^{-1}$ and various in-plane angles φ (measured from [110]). (b) Corresponding $w(B_{\text{ext}})$ plots obtained for $\mathbf{B}_{\text{ext}} \perp \mathbf{q}$. Lines are guides for the eyes. Each $w(B_{\text{ext}})$ plot is symmetric about a certain value of the external field (marked by a dotted circle) which cancels the corresponding component of the collective SO field $\mathbf{B}_{\text{SO}}^{\text{coll}}(\mathbf{q})$.

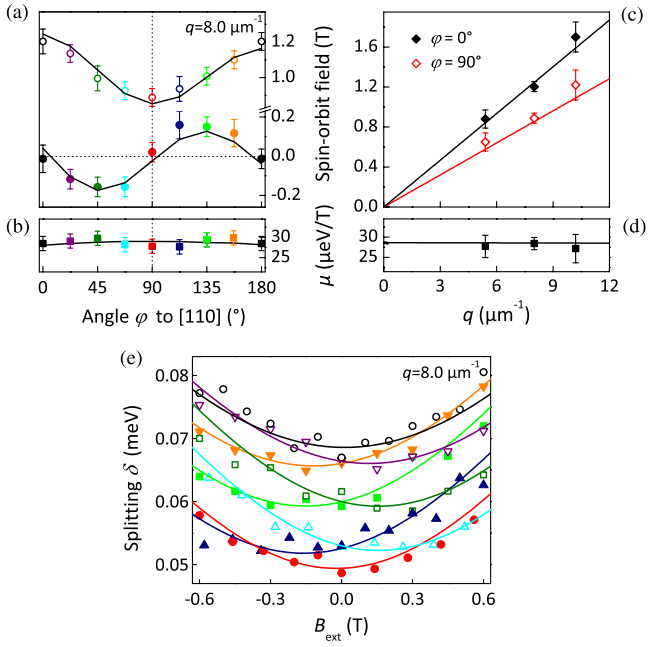

FIG. 4 (color online). SO collective field and magnetic moment. (a) Components of the collective SO field parallel ($B^{\rm coll}_{{\rm SO},\parallel}$, filled circles) and perpendicular ($B^{\rm coll}_{{\rm SO},\perp}$, open circles) to $\mathbf{q}$ for $q = 8.0\ \mu{\rm m}^{-1}$, as extracted from the data of Fig. 3, and compared with theory (lines). (b) Spin-plasmon magnetic moment μ, experimental (squares) and theoretical (line). (c) Minimum (open diamonds) and maximum (filled diamonds) SO field $|\mathbf{B}^{\rm coll}_{\rm SO}|$ versus q, compared to theoretical values (lines). (d) Spin-plasmon magnetic moment averaged over φ, experimental (squares) and theoretical (line), as a function of q. (e) Variation of the SO splitting δ with external magnetic field $\mathbf{B}_{\rm ext} \parallel \mathbf{q}$, for $q = 8.0\ \mu{\rm m}^{-1}$ (symbols, same as in Fig. 3). The experimental data are very well reproduced by Eq. (3) (lines).

($\varphi = 0°$, filled diamonds) modulus of $\mathbf{B}^{\rm coll}_{\rm SO}$. They appear proportional to q. Figure 4(d) shows the angular average of the magnetic moment μ (squares). Interestingly, μ turns out to be practically constant with q. This demonstrates that all of the SO effects are contained in $\mathbf{B}^{\rm coll}_{\rm SO}(\mathbf{q})$, and that μ is indeed the largest quantized projection of the intrinsic ISB spin-plasmon magnetic moment $\mathbf{M}$ onto the field direction. This point is confirmed by noting that $\mu \approx 2\frac{|g|\mu_{\rm B}}{2}$, that is, μ is very close to twice the magnetic moment of a single electron (when considering the g factor of bulk GaAs, $g = -0.445$). This is consistent with the fact that an ISB spin plasmon involves transitions between two spin 1/2 states, i.e., excitations of spin magnitude 1. Our results thus show that the ISB plasmon maintains the spin magnitude of a single elementary excitation, while the many-body effects are absorbed in the collective magnetic field $\mathbf{B}^{\rm coll}_{\rm SO}(\mathbf{q})$. Hence, the quantized projection of the plasmon magnetic moment can either be $\pm\mu$ [$m_\pm$ modes; see Fig. 1(c)] or 0 [$m_\parallel$ mode, whose energy is unaltered by SO coupling].

To summarize the experimental part, we validated our fine structure model by demonstrating the internal consistency of measurements—with and without magnetic field—with Eqs. (2) and (3). We emphasize again that this did not involve any adjustable parameters.

All elements are now in place to see how the collective SO magnetic field $\mathbf{B}^{\rm coll}_{\rm SO}$ emerges from the $\mathbf{k}$-dependent single-particle magnetic fields $\mathbf{B}_{\rm SO}(\mathbf{k})$ given by Eq. (1). The ISB spin plasmon is a superposition of single-particle transitions from momentum $\mathbf{k}$ in the first subband to $\mathbf{k} + \mathbf{q}$ in the empty second subband. Thus, each electron-hole pair experiences a crystal magnetic field difference $\Delta\mathbf{B}_{\rm SO}(\mathbf{k}, \mathbf{q}) = \mathbf{B}_{{\rm SO},2}(\mathbf{k} + \mathbf{q}) - \mathbf{B}_{{\rm SO},1}(\mathbf{k})$, given by

$$\frac{g\mu_{\rm B}}{2}\Delta\mathbf{B}_{\rm SO}(\mathbf{k},\mathbf{q}) = \alpha_2\begin{pmatrix} q_y \\ -q_x \end{pmatrix} + \beta_2\begin{pmatrix} q_x \\ -q_y \end{pmatrix} + (\alpha_2 - \alpha_1) \times \begin{pmatrix} k_y \\ -k_x \end{pmatrix} + (\beta_2 - \beta_1)\begin{pmatrix} k_x \\ -k_y \end{pmatrix}, \qquad (4)$$

where the subscript $n = 1, 2$ refers to the subband index. With $\alpha_1 = 3.5\ {\rm meV\,\AA}$, $\alpha_2 = 2.8\ {\rm meV\,\AA}$, $\beta_1 = 0.22\ {\rm meV\,\AA}$, and $\beta_2 = 0.79\ {\rm meV\,\AA}$, we are able to reproduce the experimental data in Figs. 2(b)–2(d) and Figs. 4(a)–4(e) in a quantitatively accurate way (see lines), using a linear-response formalism based on time-dependent density-functional theory.

$\Delta\mathbf{B}_{\rm SO}(\mathbf{k}, \mathbf{q})$ contains a $\mathbf{k}$-independent part, which is thus the same for all electron-hole pairs, and a $\mathbf{k}$-dependent part. The latter could have a disorganizing effect, causing DP dephasing. This is indeed what occurs for single-particle spin dynamics [5,8–11]. But here, the $\mathbf{k}$-dependence turns out to be exactly canceled by an additional dynamical Coulombic contribution [19], explaining how a uniform $\mathbf{B}^{\rm coll}_{\rm SO}(\mathbf{q})$ can emerge.

In a simple scenario, one could expect $\mathbf{B}^{\rm coll}_{\rm SO}(\mathbf{q})$ to be aligned with the $\mathbf{k}$-independent part of $\Delta\mathbf{B}_{\rm SO}(\mathbf{k}, \mathbf{q})$, with a slightly enhanced magnitude. But what is found is that $\mathbf{B}^{\rm coll}_{\rm SO}(\mathbf{q}) = [(2 \times 5.25)/(g\mu_{\rm B})](\overline{\alpha}q_y + \overline{\beta}q_x, -\overline{\alpha}q_x - \overline{\beta}q_y)$ (within 3%), with $\bar{\alpha} = (\alpha_1 + \alpha_2)/2$ and $\bar{\beta} = (\beta_1 + \beta_2)/2$. That is, many-body effects tilt the $\mathbf{k}$-independent part of $\Delta\mathbf{B}_{\rm SO}(\mathbf{k}, \mathbf{q})$, align it with the average single-particle SO field difference, and amplify it by a factor of about five.

Such a magnification effect due to dynamical many-body interactions is quite remarkable. At first glance, one would expect Coulomb-induced enhancements to be roughly of order r_s (Wigner-Seitz radius), which is $\simeq 1.3$ for the studied sample. On the other hand, recent experiments [25,26] suggest that the interplay of Coulomb and SO interactions could manifest in a mutual boost, leading to significant enhancement of electronic spin splittings, especially in low-dimensional systems [27].

In conclusion, we have shown that many-body effects can produce a significant departure from the single-particle picture of SO effects in crystals. In an ISB spin plasmon, despite the spread of electronic velocities, a well-organized

spin dynamics emerges at the collective level. The electrons coherently precess about a giant SO field, which gives rise to a fine structure of the spin-plasmon spectrum. This effect, which might also play a role in other helical liquids [27,28], reveals novel opportunities for magnetization control with collective SO fields.

F. B. and F. P. thank S. Majrab for technical support and B. Jusserand for fruitful discussion. F. P. acknowledges funding from C'NANO IDF 2009 (SPINWAVEDYN) and ANR 2007 (GOSPININFO). F. B. is supported by a Foundation CFM-JP Aguilar grant. I. D' A. acknowledges support from EPSRC Grant No. EP/F016719/1, and I. D' A. and F. P. acknowledge support from Royal Society Grant No. IJP 2008/R1 JP0870232. C. A. U. is supported by DOE Grant No. DE-FG02-05ER46213.

*Corresponding author: florent.baboux@insp.upmc.fr
†Present address: Centro Atómico Bariloche, Bariloche, Argentina.

[1] L. H. Thomas, Nature (London) **117**, 514 (1926).
[2] W. E. Lamb and R. C. Retherford, Phys. Rev. **79**, 549 (1950).
[3] M. I. D'yakonov and V. I. Perel', Sov. Phys. Solid State **13**, 3023 (1972).
[4] I. Žutić, J. Fabian, and S. D. Sarma, Rev. Mod. Phys. **76**, 323 (2004).
[5] V. Sih, R. C. Myers, Y. K. Kato, W. H. Lau, A. C. Gossard, and D. D. Awschalom, Nature Phys. **1**, 31 (2005).
[6] Y. K. Kato, R. C. Myers, A. C. Gossard, and D. D. Awschalom, Nature (London) **427**, 50 (2004).
[7] A. Chernyshov, M. Overby, X. Liu, J. K. Furdyna, Y. Lyanda-Geller, and L. P. Rokhinson, Nature Phys. **5**, 656 (2009).
[8] J. D. Koralek, C. P. Weber, J. Orenstein, B. A. Bernevig, S. Zhang, S. Mack, and D. D. Awschalom, Nature (London) **458**, 610 (2009).
[9] B. Das, D. C. Miller, S. Datta, R. Reifenberger, W. P. Hong, P. K. Bhattacharya, J. Singh, and M. Jaffe, Phys. Rev. B **39**, 1411 (1989).
[10] B. Jusserand, D. Richards, H. Peric, and B. Etienne, Phys. Rev. Lett. **69**, 848 (1992).
[11] L. Meier, G. Salis, I. Shorubalko, E. Gini, S. Schön, and K. Ensslin, Nature Phys. **3**, 650 (2007).
[12] R. Winkler, *Spin-Orbit Coupling Effects in Two-Dimensional Electron and Hole Systems* (Springer, Berlin, 2003).
[13] G. Dresselhaus, Phys. Rev. **100**, 580 (1955).
[14] Y. L. Bychkov and E. I. Rashba, J. Phys. C **17**, 6039 (1984).
[15] M. I. D'yakonov and V. I. Perel', Phys. Lett. **35A**, 459 (1971).
[16] A. Pinczuk, S. Schmitt-Rink, G. Danan, J. P. Valladares, L. N. Pfeiffer, and K. W. West, Phys. Rev. Lett. **63**, 1633 (1989).
[17] D. Gammon, B. V. Shanabrook, J. C. Ryan, and D. S. Katzer, Phys. Rev. B **41**, R12311 (1990).
[18] C. A. Ullrich and M. E. Flatté, Phys. Rev. B **66**, 205305 (2002).
[19] C. A. Ullrich and M. E. Flatté, Phys. Rev. B **68**, 235310 (2003).
[20] See Supplemental Material at http://link.aps.org/supplemental/10.1103/PhysRevLett.109.166401 for details on the sample fabrication, experimental setup, calculation of the spin plasmon dispersion and of the SCD linewidth.
[21] F. Perez, C. Aku-leh, D. Richards, B. Jusserand, L. C. Smith, D. Wolverson, and G. Karczewski, Phys. Rev. Lett. **99**, 026403 (2007).
[22] I. D'Amico and G. Vignale, Phys. Rev. B **62**, 4853 (2000).
[23] I. D'Amico and C. A. Ullrich, Phys. Rev. B **74**, 121303(R) (2006).
[24] C. P. Weber, N. Gedik, J. E. Moore, J. Orenstein, J. Stephens, and D. D. Awschalom, Nature (London) **437**, 1330 (2005).
[25] G. Q. Liu, V. N. Antonov, O. Jepsen, and O. K. Andersen, Phys. Rev. Lett. **101**, 026408 (2008).
[26] B. Nedniyom, R. J. Nicholas, M. T. Emeny, L. Buckle, A. M. Gilbertson, P. D. Buckle, and T. Ashley, Phys. Rev. B **80**, 125328 (2009).
[27] A. Agarwal, S. Chesi, T. Jungwirth, J. Sinova, G. Vignale, and M. Polini, Phys. Rev. B **83**, 115135 (2011).
[28] S. Raghu, S. B. Chung, X.-L. Qi, and S.-C. Zhang, Phys. Rev. Lett. **104**, 116401 (2010).